Mechanistic Insights into CO_2 Activation via Reverse Water–Gas Shift on Metal Surfaces

Luca Dietz,[†] Simone Piccinin,*[,‡] and Matteo Maestri*[,†]

[†]Laboratory of Catalysis and Catalytic Processes, Dipartimento di Energia, Politecnico di Milano, Piazza Leonardo da Vinci 32, 20133 Milano, Italy

[‡]CNR-IOM DEMOCRITOS c/o SISSA, Via Bonomea 265, 34136 Trieste, Italy

Received: December 29, 2014
Revised: January 30, 2015
Published: February 2, 2015

1. INTRODUCTION

Oil, natural gas, and coal combustion processes, involved in power generation, are accountable for increasing CO_2 atmospheric concentration, which is considered to be one of the main causes of climate changes and global warming.[1] Beside the environmental concern, CO_2 represents a highly functional and abundant chemical reagent for chemicals and fuels and could potentially be a renewable and environmentally friendly source of carbon. Therefore, upgrading CO_2 into more valuable products is considered as one of the most promising solutions for a CO_2-neutral energy supply. In this regard, cost-effective technologies are required to reduce CO_2 emissions,[2] as well as approaches where CO_2 is converted into higher-value chemicals[3] or used for the "chemical storage" of energy produced by renewable sources on a large scale.[4] In this respect, the chemical conversion of CO_2 is mainly achieved via hydrogenation to, e.g., CH_4, CH_3OH, or CH_2O on metal-based catalysts.[5−9] In these processes, a crucial issue is related to the high chemical stability of CO_2, which is hard to activate at high conversion rates and selectivity.[10] It is therefore of great importance to derive a detailed mechanistic understanding at the atomic scale to clarify the basic chemical processes of CO_2 activation, which encompasses the reverse water–gas shift (r-WGS) reaction as the first step on metal surfaces. At present, despite an increasingly large number of investigations,[11−24] debates still exist on the reaction mechanism and elementary steps involved in the water–gas shift (WGS) and r-WGS reaction pathways. In particular, three different mechanisms have been proposed for the conversion of CO_2 to CO via a r-WGS route on metal catalysts, characterized by the following key steps:[10]

$$CO_2 \rightarrow CO + O \quad (1)$$

$$CO_2 + H \rightarrow COOH \quad (2)$$

$$CO_2 + H \rightarrow HCOO \quad (3)$$

The occurrence of different mechanisms is found to depend on the specific catalysts and operating conditions. For instance, Mavrikakis and co-workers[11,12] suggested that a COOH-mediated mechanism is favored for the CO_2 hydrogenation on Pt catalysts, whereas Maestri and co-workers found—in agreement with

*E-mail: piccinin@iom.cnr.it (S.P.).
*E-mail: matteo.maestri@polimi.it (M.M.).

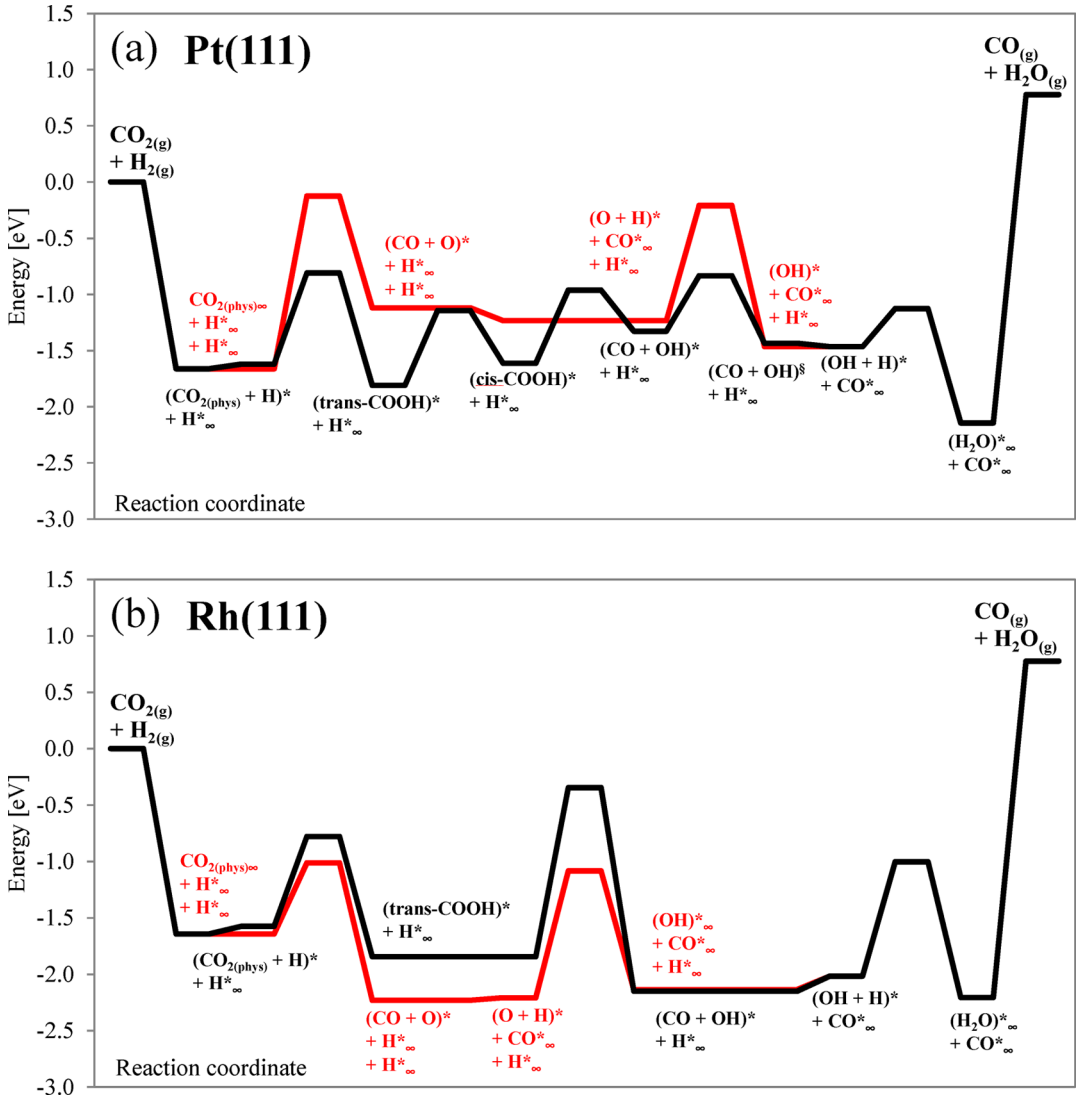

Figure 1. Dissociation (red line) and hydrogenation (black line) reaction paths on: panel (a) Pt (111); panel (b) Rh (111). The symbol "∞" means non interacting adsorbates (infinite distance) in the supercell, and the symbol "∞" is used to distinguish the "§" adsorption site from the "*" adsorption site. See Supporting Information for details.

experimental kinetic investigations[25]—that r-WGS proceeds through the CO_2 dissociation mechanism on Rh.[22,26] The formate (HCOO) mechanism—despite the fact that HCOO has been detected on the catalyst surface by the means of operando DRIFT and SSITKA analysis[17]—is usually discarded because of the high stability of HCOO on the surface, which makes HCOO a spectator rather than a reactive intermediate.[27−30]

Understanding the reasons of such mechanistic differences among the metals is crucial in the effort to gain a mechanistic interpretation of CO_2 activation, and detailed analysis by theory are required to link the different prevalent mechanisms on the metals to specific properties at the atomic scale.[31] In view of this, we present a detailed density functional theory (DFT) analysis of the dissociation mechanism ($CO_2 \rightarrow CO + O$) and the COOH-mediated mechanism for the r-WGS on (111) surfaces of Pt, Rh, Ni, Cu, Ag, and Pd. We show that the tendency of the different catalysts to promote different catalytic cycles is ultimately related to their affinity to oxygen. In particular, as O interaction with the metals weakens, the COOH-mediated mechanism becomes dominant at the expenses of the dissociation mechanism; hence, the dominant reaction path changes among the metals.

2. METHODS

All DFT calculations presented in this work are performed with the Quantum ESPRESSO code,[32] based on plane waves and ultrasoft pseudopotentials. The exchange and correlation potential is approximated using the generalized-gradient approximation as formulated by Perdew, Burke, and Ernzerhof (GGA-PBE) functional.[33,34] Kohn−Sham states are expanded in a basis set of plane waves with a cutoff of 40 Ry and a $6 \times 6 \times 1$ Monkhorst−Pack grid is used to sample the Brillouin zone. This set of parameters was verified to ensure the numerical convergence within 30 meV of the computed binding energies. The (111) metal surfaces are modeled with a periodically repeated slab geometry, using a 2×2 surface unit cell, four atomic layers, and a vacuum spacing of 12 Å. Metal surfaces are characterized by very small relaxation.[35] Therefore, we keep the first three layers fixed at the atomic bulk position, whereas the fourth layer is allowed to relax. Adsorption is allowed only on one side of the slab. Binding energies are computed as the difference between the energy of the adsorption system (i.e., slab with adsorbate) and the sum of the energies of the clean metal slab and of the gas-phase molecule.

Spin-polarized calculations are employed for gas-phase molecules as well as for the Ni surfaces, which display ferromagnetic behavior.[36] Activation energies are computed by means of the Climbing Image-Nudged Elastic Band (CI-NEB) method,[37] using 12 images and a convergence criterion on forces of 0.1 eV/Å. Since the GGA-PBE functional does not describe van der Waals (vdW) interactions, we use the Grimme approach[38] to account for their influence on the activation energies. As reported in the Supporting Information, inclusion of dispersion interactions leads to a slight and almost rigid shift of all activation energies, without significantly altering their relative magnitude. In our work the transition state (TS) is located without the inclusion of vdW interactions. The initial and final states are later optimized accounting for vdW effects, and the energy of the TS is refined with a single-point (i.e., fixed ions) calculation including vdW effects. As shown in the Supporting Information, this procedure differs negligibly from a NEB calculation in which vdW effects are accounted for also in the search of the TS.

3. RESULTS AND DISCUSSION

We start with the analysis of the dissociation and COOH-mediated mechanisms on Pt(111) and Rh(111) surfaces (Figure 1). Details on the elementary steps included in the two mechanisms are reported in Table 1. For additional information on the reaction pathways, we refer the reader to the Supporting Information.

Table 1. Dissociation and COOH-Mediated Mechanisms

dissociation	COOH-mediated
1. $CO_2^* + * \rightarrow CO^* + O^*$	1. $CO_2^* + H^* \rightarrow$ trans-COOH* + *
2. $O^* + H^* \rightarrow OH^* + *$	2. trans-COOH* $\rightarrow$ cis-COOH*
3. $OH^* + H^* \rightarrow H_2O^* + *$	3. cis-COOH* + * $\rightarrow$ CO* + OH*
	4. $OH^* + H^* \rightarrow H_2O^* + *$

In the case of Pt (Figure 1a), upon adsorption of CO_2 and H_2 at the surface, the hydrogenation of CO_2 to trans-COOH turns out to be more favorable than the dissociation of CO_2 (0.81 vs 1.54 eV), in agreement with that reported also by Mavrikakis and co-workers.[11] In the case of Rh (Figure 1b), instead, the dissociation route prevails because it exhibits an activation energy considerably lower than the one needed for the formation of the trans-COOH (0.63 vs 0.80 eV). In particular, on one hand, the barrier for the formation of trans-COOH is not markedly affected by the metal (0.81 and 0.80 eV for Pt and Rh, respectively). On the other hand, a remarkable decrease of the barrier for the CO_2 dissociation is predicted (1.54 and 0.63 eV for Pt and Rh, respectively). Such a change is crucial in enabling two different mechanisms for CO_2 activation on the two metals as reported in Figure 1a,b.

Figure 2 reports the comparison between the dissociation and hydrogenation activation barriers for all the six investigated metals. Ni and Cu show behavior similar to Rh, with the dissociation route favored on the hydrogenation one. Ag and Pd, in contrast, are similar to Pt and the hydrogenation route turns out to be less activated than the dissociation one. We now aim to rationalize such a trend among the metals and to relate it to specific properties at the atomistic level, which can then be eventually used to identify a proper catalyst descriptor. To this end, we first focus our attention on the CO_2 dissociation reaction.

3.1. CO_2 Dissociation Pathway. As previously reported in the literature,[39,40] CO_2 displays a weak interaction with all the

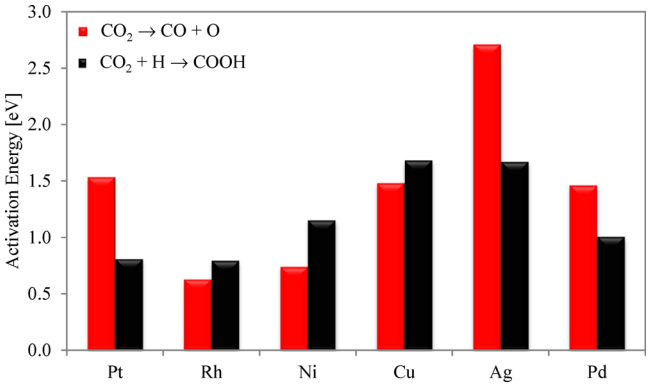

Figure 2. Dissociation (red bars) and hydrogenation (black bars) activation energies on Pt(111), Rh(111), Ni(111), Cu(111), Ag(111), and Pd(111) metals.

metal surfaces. Starting from CO_2 as initial state, we computed the minimum energy path for the dissociation into CO and O adsorbed in neighboring top and fcc sites of the (111) surface, respectively. For Pt, Rh, and Ni metal surfaces we found the reaction to proceed through a less energetically favored metastable intermediate, where CO_2 is bent and the C−O bonds stretched.[40]

As Figure 3 clearly shows, the geometry of the transition state is nearly identical for all the metals. The TS of the reaction is characterized by a fully cleaved C−O bond, and a second

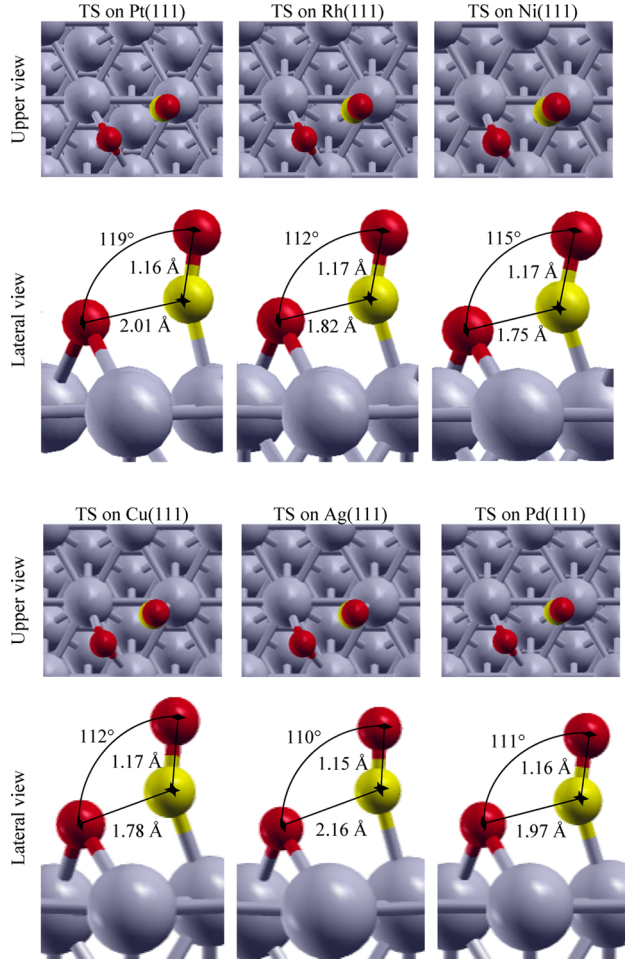

Figure 3. Lateral and upper view of the transition-state structure for the dissociation reaction on the different metals.

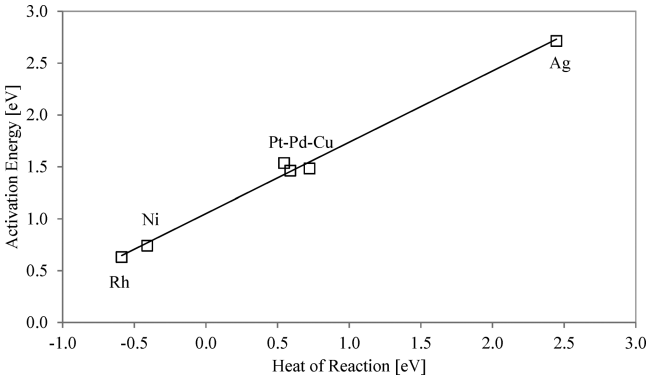

Figure 4. Brønsted–Evans–Polanyi (BEP) relation for the CO_2 dissociation reaction ($CO_2 \rightarrow CO + O$). Fitting model: y = 0.6868x + 1.0502; R^2 = 0.9935.

C–O bond that in all cases is almost identical to the value for the CO molecule in the final state (~1.15 Å). At the TS, the O atom is in a bridge position, while the CO molecule is slightly tilted and displaced away from the hollow site toward the top site. In spite of very similar geometries, the activation energy for this reaction is remarkably different on the six metals, from 0.63 eV for Rh to 2.71 eV for Ag.

The reaction closely obeys the Brønsted–Evans–Polanyi (BEP) relation[41−43] since there is a linear relationship between the activation energy and the energy of reaction as shown in Figure 4. From the magnitude of the linear coefficient in Figure 4 (0.69), we can infer that the TS for this step is of late character, consistent with the geometries shown in Figure 3 and with the fact that the binding energy of CO_2 (the initial state of this reaction) is very similar and weak on all the metals. Therefore, the energy of the TS is strongly influenced by the energy of the final state, and in particular by O. In fact, as shown in Figure 5, the trend of the activation energy for the CO_2 dissociation among the metals turns out to be mostly correlated with the O binding energy.

Consequently, any sort of destabilization suffered by O on the surface has a direct effect upon the capability of the system to dissociate CO_2 into CO and O. To further assess the latter point, we computed the activation energy of the dissociation reaction at different coverages, which can significantly affect the binding energy of the adsorbates and, in turn, the dissociation energy.[44] As an example, we report in Figure 6 the effect of oxygen and hydrogen coverage on the dissociation on Cu. On one hand, the interaction of CO_2 with the surface turns out to be not affected by the higher coverage, given the weak interaction between CO_2 and the surface. On the other hand,

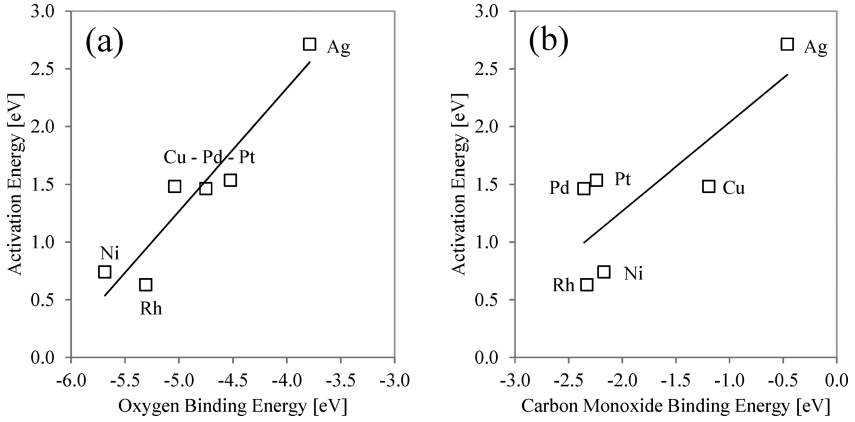

Figure 5. Correlation between the forward activation energy of the dissociation reaction ($CO_2 \rightarrow CO + O$) and: panel (a) oxygen binding energy (fitting model: y = 1.0648x + 6.5919; R^2 = 0.8956); panel (b) carbon monoxide binding energy (fitting model: y = 0.7666x + 2.8024; R^2 = 0.6534).

Table 2. Species Binding Energies

	Pt(111)		Rh(111)		Ni(111)	
metal species	BE [eV]	site	BE [eV]	site	BE [eV]	site
CO_2	−0.51	equivalent	−0.32	equivalent	−0.27	equivalent
$CO_{2\ metastable}$	−0.19	top	−0.11	top	−0.07	top
CO	−2.24	hcp	−2.33	hcp	−2.17	hcp
O	−4.52	fcc	−5.31	fcc	−5.69	fcc
H	−2.85	fcc	−2.93	fcc	−2.87	fcc
trans-COOH	−3.13	top	−3.08	top	−2.80	top
cis-COOH	−3.01	top	−2.71	top	−2.55	top
	Cu(111)		Ag(111)		Pd(111)	
metal species	BE [eV]	site	BE [eV]	site	BE [eV]	site
CO_2	−0.21	equivalent	−0.26	equivalent	−0.33	equivalent
$CO_{2\ metastable}$						
CO	−1.19	fcc	−0.46	top	−2.36	hcp
O	−5.04	fcc	−3.79	fcc	−4.75	fcc
H	−2.58	fcc	−2.18	fcc	−2.95	fcc
trans-COOH	−2.12	top	−1.59	top	−2.74	top
cis-COOH	−2.02	top	−1.18	top	−2.58	top

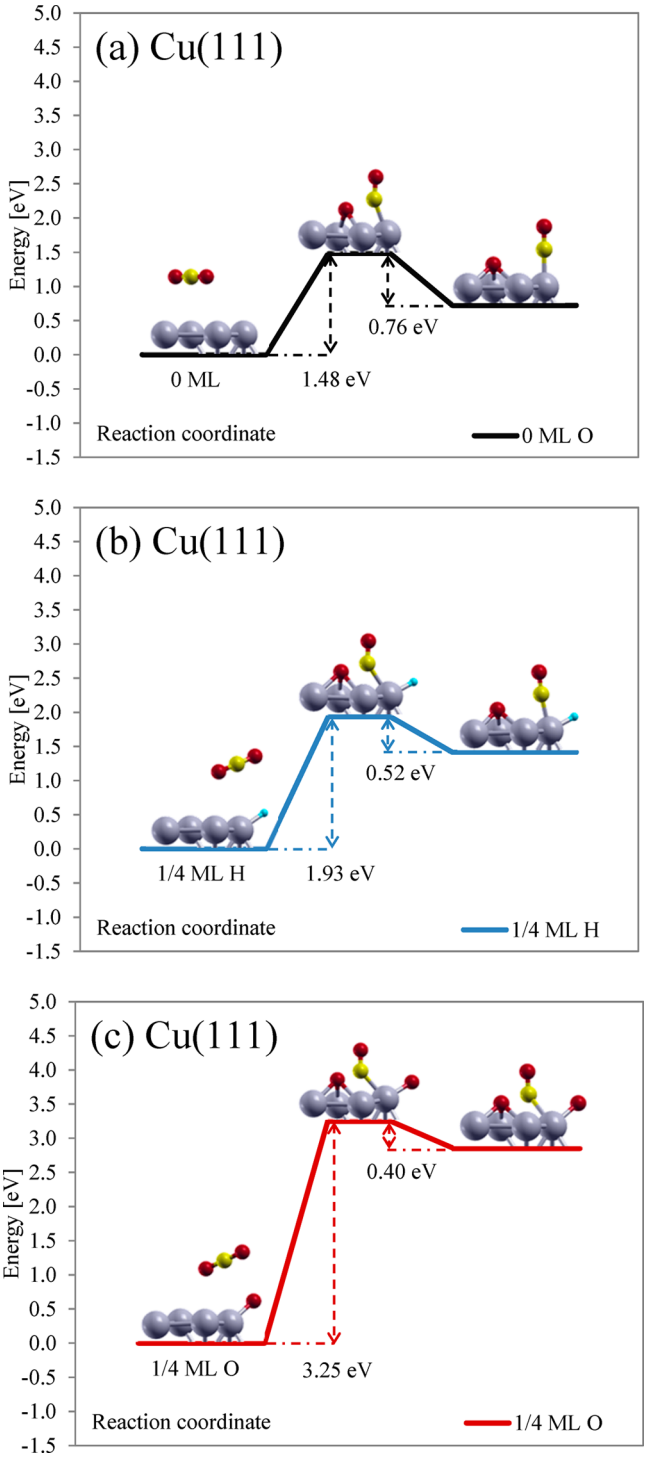

Figure 6. Activation energy of the dissociation step on Cu(111): (a) 0 ML, (b) 1/4 ML of adsorbed hydrogen, and (b) 1/4 ML of adsorbed oxygen.

both higher hydrogen (Figure 6b) and oxygen (Figure 6c) coverage causes an intense repulsion for O and thus a destabilization of the final state of the reaction with respect to the case of a clean metal slab (Figure 6a). As a result, the dissociation reaction becomes more endothermic. Given the late character of the TS, the destabilization of the final state on the surface results in a destabilization of the transition state too and, correspondingly, the activation energy increases, as evident by comparing the results obtained when CO_2 dissociates on a clean metal slab with those obtained when both 1/4 ML H and 1/4 ML O coverages are present.

It is important to note that when the differences between the two competing pathways are small (as in the case of Cu) coverage effects may play a crucial role in determining the dominant reaction mechanism. For instance, by considering 1/4 ML H coverage on Cu, CO_2 dissociation becomes more activated (1.93 eV) than hydrogenation (1.69 eV).

3.2. CO_2 Hydrogenation to trans-COOH. We now consider the hydrogenation route to trans-COOH, which is the competitive pathway with respect to the dissociation reaction. In sharp contrast with the dissociation pathway, CO_2 hydrogenation to trans-COOH displays much less marked differences among the metals in terms of activation energy.

Atomic hydrogen binds preferentially in a hollow site on all six metals, with a slight preference for the fcc site over the hcp site in all cases (see Table 2). As initial state for the CO_2 hydrogenation reaction, we hence selected a configuration with a H atom occupying a fcc site and CO_2 weakly interacting with the metal surfaces. As final state of this reaction we consider the trans-COOH species, adsorbed through the C atom at a top site. In contrast to what is observed for the dissociation route, we find that—despite the same initial and final configurations—the geometry of the minimum energy path (MEP) for CO_2 hydrogenation changes among the different metals. For instance, in the case of Pt, H diffuses to the top site before reacting with CO_2. On the Rh surface, instead, the H atom migrates toward the bridge site without going through the top site. Consequently, the geometry of TS varies among the different metals, as shown in Figure 7.

The different MEP and the different TS among the metals are the results of the different contributions of reactants and products to the TS. In particular, in contrast to the CO_2 dissociation reaction, initial state for the hydrogenation path shows a non-negligible interaction with the surface due to the presence of H, as evident from the values of H binding energies reported in Table 2. In this situation, the formation of the TS is affected both by H (reactant) and trans-COOH (product). As a first approximation, the relative difference between the binding energies of reactants and products can provide an estimation of the importance of reactants and products in determining the nature of the TS. Let us consider for instance the cases of Rh and Cu. On one hand, by going from Rh to Cu (see Table 2), trans-COOH becomes 0.96 eV less stable, while H gets destabilized of 0.35 eV. On the other hand, CO_2 interacts weakly with the surface in both cases. Consequently, the energy cost to form the TS becomes less dominated by trans-COOH by going from Rh to Cu, and thus the character of the TS is more "early" (i.e., strongly influenced by the reactants) for Rh than for Cu, as a result of the different interactions of reactants and products with the metal surface. This is consistent with the TS geometries reported in Figure 7. The TS on Cu resembles more the initial state (H and CO_2), whereas on Rh the TS has a geometry that is more similar to the product (trans-COOH). For instance, for Rh, the C−metal distance is almost identical to the value in trans-COOH in the final state (2.01 vs 1.98 Å), whereas, for Cu, the C−metal distance is quite different from its value in trans-COOH in the final state (2.34 vs 1.95 Å). As a consequence of this change in the nature of the TS among the metals, the reaction does not closely obey the BEP principle, as shown in Figure 8.

Consequently, a simple descriptor of the catalytic activity via the hydrogenation mechanism cannot be identified.

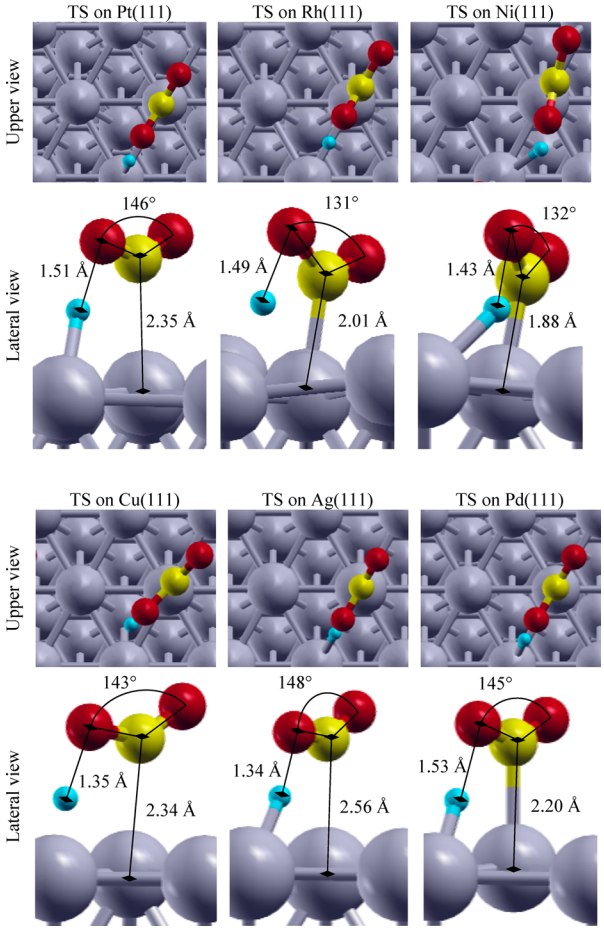

Figure 7. Lateral and upper view of the transition-state structure for the hydrogenation reaction on the different metals.

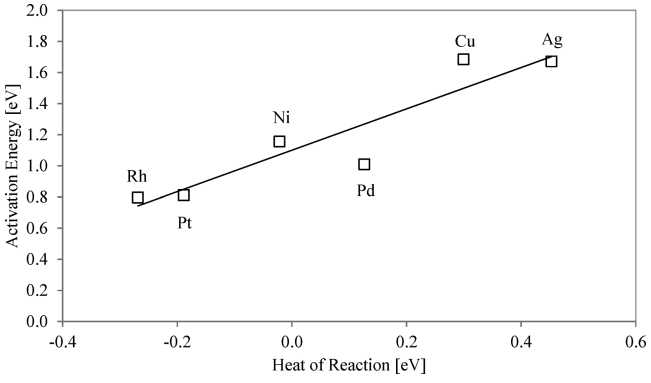

Figure 8. Brønsted–Evans–Polanyi (BEP) relation for the CO_2 hydrogenation reaction (CO_2 + H → COOH). Fitting model: y = 1.3294x + 1.1004; R^2 = 0.8587.

3.3. Comparison between CO_2 Dissociation and COOH-Mediated Mechanisms. On the whole, our analysis pointed out that the dissociation reaction is strongly affected by the O–metal interactions, whereas the hydrogenation pathway is neither directly related to any specific adsorbate–metal interaction nor strongly affected by the metal. As a consequence of these conclusions, the difference in the activation energies for the dissociation and the hydrogenation paths is found to be correlated with the binding energy of oxygen, by following the trend of the CO_2 dissociation with respect to O binding energy. This is shown in Figure 9.

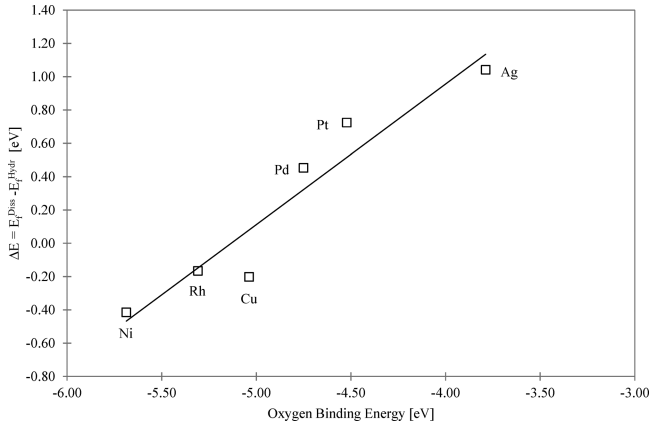

Figure 9. Correlation between the binding energy of oxygen and difference of the activation energies for the dissociation and hydrogenation reactions. Fitting model: y = 0.8436x + 4.3307; R^2 = 0.9114.

As a result, on one hand, more oxophilic surfaces will favor the dissociation mechanism; on the other hand, less oxophilic surfaces will favor the hydrogenation route. All in all, the difference in the two activation energies is well captured by this simple descriptor, which can then be used to discriminate which of the two mechanisms is dominant on the different metals.

4. CONCLUSIONS

By means of a systematic DFT analysis of the r-WGS reaction on Pt(111), Rh(111), Ni(111), Cu(111), Ag(111), and Pd(111) surfaces, we have provided compelling evidence that the change in affinity to oxygen among the different metals is the main cause to enable different dominant pathways for the CO_2 activation. In particular, COOH-mediated mechanism is favored on Pt, Ag, and Pd, whereas Rh, Ni, and Cu dissociate CO_2 to CO and O, thus making the dissociation mechanism prevalent. We found that such a difference is related to a drastic change in the CO_2 dissociation barrier, which is not compensated by an equivalent variation in the hydrogenation activation energy. On one hand, due to the late character of the transition state for the dissociation reaction and the very weak interaction of the CO_2 molecule with all the surfaces, the nature of the interaction between the adsorbed O and the surface is crucial in dictating the height of the CO_2 dissociation barrier. Specifically, the stronger the metal–O interaction, the lower the CO_2 dissociation barrier, thus making the dissociation route more favorable over the competing hydrogenation route, which was found to be markedly less affected by the metal surface. As a result, the dominant reaction pathway for r-WGS changes among the metals. We found that the binding energy of oxygen scales almost linearly with the difference between the activation energy of the two competing paths, and therefore this quantity can be used as a simple descriptor to discriminate which of the two mechanisms is dominant on different metals.

ASSOCIATED CONTENT

Supporting Information

This material is available free of charge via Internet.

Notes

The authors declare no competing financial interest.

ACKNOWLEDGMENTS

Computational time at CINECA-Fermi (Bologna, Italy) is gratefully acknowledged.

REFERENCES

(1) Cox, P. M.; Betts, R. A.; Jones, C. D.; Spall, S. A.; Totterdell, I. J. Acceleration of Global Warming due to Carbon-Cycle Feedbacks in a Coupled Climate Model. *Nature* **2000**, *408*, 184−187.

(2) Song, C. Global Challenges and Strategies for Control, Conversion and Utilization of CO_2 for Sustainable Development Involving Energy, Catalysis, Adsorption and Chemical Processing. *Catal. Today* **2006**, *115*, 2−32.

(3) Olah, G. A.; Goeppert, A.; Prakash, G. K. S. Chemical Recycling of Carbon Dioxide to Methanol and Dimethyl Ether: From Greenhouse Gas to Renewable, Environmentally Carbon Neutral Fuels and Synthetic Hydrocarbons. *J. Org. Chem.* **2009**, *74*, 487−498.

(4) Jentsch, M.; Trost, T.; Sterner, M. Optimal Use of Power-to-Gas Energy Storage Systems in an 85% Renewable Energy Scenario. *Energy Procedia* **2014**, *46*, 254−261.

(5) Cai, M.; Wen, J.; Chu, W.; Cheng, X.; Li, Z. Methanation of Carbon Dioxide on Ni/ZrO_2-Al_2O_3 Catalysts: Effects of ZrO_2 Promoter and Preparation Method of Novel ZrO_2-Al_2O_3 Carrier. *J. Nat. Gas Chem.* **2011**, *20*, 318−324.

(6) Chang, F.-W.; Kuo, M.-S.; Tsay, M.-T.; Hsieh, M.-C. Hydrogenation of CO_2 over Nickel Catalysts on Rice Husk Ash-Alumina Prepared by Incipient Wetness Impregnation. *Appl. Catal., A* **2003**, *247*, 309−320.

(7) Karelovic, A.; Ruiz, P. CO_2 Hydrogenation at Low Temperature over Rh/γ-Al_2O_3 Catalysts: Effect of the Metal Particle Size on Catalytic Performances and Reaction Mechanism. *Appl. Catal., B* **2012**, *113*−*114*, 237−249.

(8) Yu, K.-P.; Yu, W.-Y.; Kuo, M.-C.; Liou, Y.-C.; Chien, S.-H. Pt/titania-Nanotube: A Potential Catalyst for CO_2 Adsorption and Hydrogenation. *Appl. Catal., B* **2008**, *84*, 112−118.

(9) Studt, F.; Abild-Pedersen, F.; Varley, J. B.; Nørskov, J. K. CO and CO_2 Hydrogenation to Methanol Calculated Using the BEEF-vdW Functional. *Catal. Lett.* **2012**, *143*, 71−73.

(10) Cheng, D.; Negreiros, F. R.; Aprà, E.; Fortunelli, A. Computational Approaches to the Chemical Conversion of Carbon Dioxide. *ChemSusChem* **2013**, *6*, 944−965.

(11) Grabow, L. C.; Gokhale, A. A.; Evans, S. T.; Dumesic, J. A.; Mavrikakis, M. Mechanism of the Water Gas Shift Reaction on Pt: First Principles, Experiments, and Microkinetic Modeling. *J. Phys. Chem. C* **2008**, *112*, 4608−4617.

(12) Gokhale, A. A.; Dumesic, J. A.; Mavrikakis, M. On the Mechanism of Low-Temperature Water Gas Shift Reaction on Copper. *J. Am. Chem. Soc.* **2008**, *130*, 1402−1414.

(13) Grabow, L. C.; Mavrikakis, M. Mechanism of Methanol Synthesis on Cu through CO_2 and CO Hydrogenation. *ACS Catal.* **2011**, *1*, 365−384.

(14) Peng, G.; Sibener, S. J.; Schatz, G. C.; Mavrikakis, M. CO_2 Hydrogenation to Formic Acid on Ni(110). *Surf. Sci.* **2012**, *606*, 1050−1055.

(15) Yang, Y.; Mims, C. A.; Mei, D. H.; Peden, C. H. F.; Campbell, C. T. Mechanistic Studies of Methanol Synthesis over Cu from $CO/CO_2/H_2/H_2O$ Mixtures: The Source of C in Methanol and the Role of Water. *J. Catal.* **2013**, *298*, 10−17.

(16) Hong, Q.-J.; Liu, Z.-P. Mechanism of CO_2 Hydrogenation over $Cu/ZrO_2(2\bar{1}2)$ Interface from First-Principles Kinetics Monte Carlo Simulations. *Surf. Sci.* **2010**, *604*, 1869−1876.

(17) Meunier, F. C.; Tibiletti, D.; Goguet, A.; Shekhtman, S.; Hardacre, C.; Burch, R. On the Complexity of the Water-Gas Shift Reaction Mechanism over a Pt/CeO_2 Catalyst: Effect of the Temperature on the Reactivity of Formate Surface Species Studied by Operando DRIFT during Isotopic Transient at Chemical Steady-State. *Catal. Today* **2007**, *126*, 143−147.

(18) Kalamaras, C. M.; Panagiotopoulou, P.; Kondarides, D. I.; Efstathiou, A. M. Kinetic and Mechanistic Studies of the Water−Gas Shift Reaction on Pt/TiO_2 Catalyst. *J. Catal.* **2009**, *264*, 117−129.

(19) Jacobs, G.; Davis, B. H. Reverse Water-Gas Shift Reaction: Steady State Isotope Switching Study of the Reverse Water-Gas Shift Reaction Using in Situ DRIFTS and a Pt/ceria Catalyst. *Appl. Catal., A* **2005**, *284*, 31−38.

(20) Kalamaras, C. M.; Americanou, S.; Efstathiou, A. M. Redox" vs "associative Formate with −OH Group Regeneration" WGS Reaction Mechanism on Pt/CeO_2: Effect of Platinum Particle Size. *J. Catal.* **2011**, *279*, 287−300.

(21) Stamatakis, M.; Chen, Y.; Vlachos, D. G. First-Principles-Based Kinetic Monte Carlo Simulation of the Structure Sensitivity of the Water−Gas Shift Reaction on Platinum Surfaces. *J. Phys. Chem. C* **2011**, *115*, 24750−24762.

(22) Maestri, M.; Reuter, K. Molecular-Level Understanding of WGS and Reverse WGS Reactions on Rh through Hierarchical Multiscale Approach. *Chem. Eng. Sci.* **2012**, *74*, 296−299.

(23) Liu, C.; Cundari, T. R.; Wilson, A. K. CO_2 Reduction on Transition Metal (Fe, Co, Ni, and Cu) Surfaces: In Comparison with Homogeneous Catalysis. *J. Phys. Chem. C* **2012**, *116*, 5681−5688.

(24) Wang, G.-C.; Nakamura, J. Structure Sensitivity for Forward and Reverse Water-Gas Shift Reactions on Copper Surfaces: A DFT Study. *J. Phys. Chem. Lett.* **2010**, *1*, 3053−3057.

(25) Donazzi, A.; Beretta, A.; Groppi, G.; Forzatti, P. Catalytic Partial Oxidation of Methane over a 4% Rh/α-Al_2O_3 Catalyst Part II: Role of CO_2 Reforming. *J. Catal.* **2008**, *255*, 259−268.

(26) Maestri, M.; Livio, D.; Beretta, A.; Groppi, G. Hierarchical Refinement of Microkinetic Models: Assessment of the Role of the WGS and R-WGS Pathways in CH_4 Partial Oxidation on Rh. *Ind. Eng. Chem. Res.* **2014**, *53*, 10914−10928.

(27) Peng, G.; Sibener, S. J.; Schatz, G. C.; Ceyer, S. T.; Mavrikakis, M. CO_2 Hydrogenation to Formic Acid on Ni(111). *J. Phys. Chem. C* **2012**, *116*, 3001−3006.

(28) Pekridis, G.; Kalimeri, K.; Kaklidis, N.; Vakouftsi, E.; Iliopoulou, E. F.; Athanasiou, C.; Marnellos, G. E. Study of the Reverse Water Gas Shift (RWGS) Reaction over Pt in a Solid Oxide Fuel Cell (SOFC) Operating under Open and Closed-Circuit Conditions. *Catal. Today* **2007**, *127*, 337−346.

(29) Chen, C.; Cheng, W.; Lin, S. Mechanism of CO Formation in Reverse Water − Gas Shift Reaction over Cu/Al_2O_3 Catalyst. *Catal. Lett.* **2000**, *68*, 45−48.

(30) Vesselli, E.; Rizzi, M.; De Rogatis, L.; Ding, X.; Baraldi, A.; Comelli, G.; Savio, L.; Vattuone, L.; Rocca, M.; Fornasiero, P.; et al. Hydrogen-Assisted Transformation of CO_2 on Nickel: The Role of Formate and Carbon Monoxide. *J. Phys. Chem. Lett.* **2010**, *1*, 402−406.

(31) Clay, J. P.; Greeley, J. P.; Ribeiro, F. H.; Nicholas Delgass, W.; Schneider, W. F. DFT Comparison of Intrinsic WGS Kinetics over Pd and Pt. *J. Catal.* **2014**, *320*, 106−117.

(32) Giannozzi, P.; Baroni, S.; Bonini, N.; Calandra, M.; Car, R.; Cavazzoni, C.; Ceresoli, D.; Chiarotti, G. L.; Cococcioni, M.; Dabo, I.; et al. QUANTUM ESPRESSO: A Modular and Open-Source Software Project for Quantum Simulations of Materials. *J. Phys.: Condens. Matter* **2009**, *21*, 395502.

(33) Perdew, J. P.; Chevary, J. A.; Vosko, S. H.; Jackson, K. A.; Pederson, M. R.; Singh, D. J.; Fiolhais, C. Atoms, Molecules, Solids, and Surfaces: Applications of the Generalized Gradient Approximation for Exchange and Correlation. *Phys. Rev. B* **1992**, *46*, 6671−6687.

(34) Vanderbilt, D. Soft Self-Consistent Pseudopotentials in a Generalized Eigenvalue Formalism. *Phys. Rev. B* **1990**, *41*, 7892−7895.

(35) Singh-Miller, N. E.; Marzari, N. Surface Energies, Work Functions, and Surface Relaxations of Low-Index Metallic Surfaces from First Principles. *Phys. Rev. B* **2009**, *80*, 235407.

(36) Slater, J. The Ferromagnetism of Nickel. *Phys. Rev.* **1936**, *49*, 537−545.

(37) Henkelman, G.; Uberuaga, B. P.; Jónsson, H. A Climbing Image Nudged Elastic Band Method for Finding Saddle Points and Minimum Energy Paths. *J. Chem. Phys.* **2000**, *113*, 9901.
(38) Grimme, S. Semiempirical GGA-Type Density Functional Constructed with a Long-Range Dispersion Correction. *J. Comput. Chem.* **2006**, *27*, 1787−1799.
(39) Solymosi, F. The Bonding, Structure and Reactions of CO_2 Adsorbed on Clean and Promoted Metal Surfaces. *J. Mol. Catal.* **1991**, *65*, 337−358.
(40) Wang, S.-G.; Liao, X.-Y.; Cao, D.-B.; Huo, C.-F.; Li, Y.-W.; Wang, J.; Jiao, H. Factors Controlling the Interaction of CO_2 with Transition Metal Surfaces. *J. Phys. Chem. C* **2007**, *111*, 16934−16940.
(41) Logadottir, A.; Rod, T. H.; Nørskov, J. K.; Hammer, B.; Dahl, S.; Jacobsen, C. J. H. The Brønsted−Evans−Polanyi Relation and the Volcano Plot for Ammonia Synthesis over Transition Metal Catalysts. *J. Catal.* **2001**, *197*, 229−231.
(42) Bligaard, T.; Nørskov, J. K.; Dahl, S.; Matthiesen, J.; Christensen, C. H.; Sehested, J. The Brønsted−Evans−Polanyi Relation and the Volcano Curve in Heterogeneous Catalysis. *J. Catal.* **2004**, *224*, 206−217.
(43) Gong, X.-Q.; Liu, Z.-P.; Raval, R.; Hu, P. A Systematic Study of CO Oxidation on Metals and Metal Oxides: Density Functional Theory Calculations. *J. Am. Chem. Soc.* **2004**, *126*, 8−9.
(44) Bleakley, K.; Hu, P. A Density Functional Theory Study of the Interaction between CO and O on a Pt Surface: CO/Pt(111), O/Pt(111), and CO/O/Pt(111). *J. Am. Chem. Soc.* **1999**, *121*, 7644−7652.